Available online at www.sciencedirect.com

SciVerse ScienceDirect

Ceramics International 38 (2012) 2983–2989

CERAMICS INTERNATIONAL

www.elsevier.com/locate/ceramint

Thermal cyclic life and failure mechanism of nanostructured 13 wt%Al_2O_3 doped YSZ coating prepared by atmospheric plasma spraying

Lei Jin, Liyong Ni, Qinghe Yu, Abdul Rauf, Chungen Zhou *

Department of Materials Science and Engineering, Beijing University of Aeronautics and Astronautics, Key Laboratory of Aerospace Materials and Performance (Ministry of Education), Beijing 100191, China

Received 12 October 2011; received in revised form 28 November 2011; accepted 29 November 2011
Available online 7 December 2011

Abstract

Nanostructured 13 wt%Al_2O_3 doped nanostructured 8 wt% yttria stabilized zirconia (nano-13AlYSZ) coatings were deposited by atmospheric plasma spray (APS). The isothermal oxidation and thermal cyclic life of the nano-13AlYSZ coating at 1100 °C were investigated. The isothermal oxidation test results indicate that the oxidation kinetics of nano-13AlYSZ follows a parabolic law. The parabolic rate constant at 1100 °C is calculated 0.04365 $mg^2\ cm^{-4}\ h^{-1}$. The thermal cyclic life of nano-13AlYSZ coating is about 953 times at 1100 °C. The failure of the nano-13AlYSZ coating occurs at the interface between the nano-13AlYSZ coating and the thermal growth oxide (TGO). A finite element method is employed to analyze the stress distribution in the nano-13AlYSZ coating. The results show that maximum stresses occur at the top coat/TGO interface.

Keywords: Atmospheric plasma spraying; Nanostructured Al_2O_3–Y_2O_3–ZrO_2; Thermal cyclic life; Finite element method

1. Introduction

Nanostructured yttria stabilized zirconia coatings (nano-YSZ) have received wide interest because of their low thermal conductivity, high coefficient of thermal expansion, excellent thermodynamic and mechanical properties in the turbine environment [1–7]. However, the grain growth and the phase instability during annealing [8–11], and consequently the disappearance of the nanostructure during sintering process, severely weaken the thermal and mechanical properties of the coatings. In order to improve the thermal and mechanical properties, nanostructured coatings have been modified by doping with several additives, such as Al_2O_3 [12,13], La_2O_3 and HfO_2 [14–16]. In our previous work, the microstructure and thermal physical properties of nanostructured Al_2O_3-YSZ coatings have been studied. It is shown that the addition of nano-sized Al_2O_3 effectively inhibits the grain growth of the ZrO_2 phase leading to the high thermal stability at high temperature [17]. Meanwhile, the addition of Al_2O_3 has a great influence on decreasing the thermal conductivity of nano-YSZ [18]. During the high temperature service, a thermally grown oxide (TGO) forms at the bond coat/top coat interface. The TGO plays an important role in the failure of thermal barrier coatings due to the grain growth, cracks always occurs between the interface of top coat/TGO or bond coat/TGO when the stresses is large enough. The stresses produced during the thermal cyclic process result in the spallation of the top coating when it is large enough. Therefore, the stress is the main reason for the thermal barrier coating failure. A transient thermal structural finite element solution was employed to analyze the stress distribution in the nano-YSZ and traditional YSZ coatings. However, the failure mechanism of the nanostructured Al_2O_3 doped YSZ coating during the thermal cycling process is rarely reported.

With the above background, the objective is to study the isothermal oxidation behavior and thermal cycling life of the nano-Al_2O_3 doped nano-YSZ coating. For the purpose of quantitative determination of the stress states in the nano-Al_2O_3 doped YSZ coating as it cools in air, finite element method is employed to model the coating. In addition, the failure mechanism of the nanostructured Al_2O_3-YSZ coating has been explored.

* Corresponding author. Tel.: +86 10 82338622; fax: +86 10 82338200.
E-mail address: cgzhou@buaa.edu.cn (C. Zhou).

0272-8842/$36.00
doi:10.1016/j.ceramint.2011.11.077

2. Experimental procedure

2.1. Preparation of TBCs

Commercially available nano-YSZ (8 wt% yttria stabilized zirconia) and nano-Al_2O_3 powders (Nanjing High Technology Nano Company of China) were used as starting materials. The average sizes of nano-YSZ and nano-Al_2O_3 particles were 30 nm and 20 nm, respectively. Mixtures of 13 wt%Al_2O_3–87 wt%YSZ (13AlYSZ) were mixed and reconstituted into spherical micrometer-sized granules (typical size range in 30–100 μm) by spray-drying process. For comparison, the nano-13AlYSZ and conventional YSZ coating with the same thicknesses of bond coat and ceramic layer were produced under the same plasma spraying parameters. The parameters for plasma spraying bond coat and top coat are shown in Table 1.

2.2. Cyclic oxidation

For thermal cycling test, the substrates were cut into coupons with a dimension of 15 mm × 10 mm × 3 mm from a wrought sheet of nickel-based superalloy with nominal composition (wt%) of Ni–5Co–10Cr–4Mo–5W–3.5Al–2Ti–2Nb (K3). In order to improve the adherence of the coating, these coupons were grit-blasted, using 250-μm alumina grit, to obtain a sharp-peaked surface contour with a roughness average of 4–5 μm. The coupons were coated with a NiCrAlY bond coat to a thickness of about 100 μm. A top coat of nano-13AlYSZ was deposited on the substrate to a thickness of about 200 μm using APS process.

Furnace cycle tests were performed under atmospheric pressure using a tube type furnace. The average heating rate was 10 °C/min from room temperature to 1100 °C. The samples were firstly heated at 1100 °C for 50 min, and then force cooled by an air fan for 10 min to ambient temperature. The lifetime of the coatings were defined by the cycle numbers at which 5% of total coating surface area was spalled or delaminated.

2.3. Isothermal oxidation

For isothermal oxidation test, the samples were coated on all sides and the isothermal oxidation tests were carried out at 1100 °C for 147 h in static air. The specimens were placed in alumina crucibles, oxidized at 1100 °C and then cooled to room temperature at regular intervals for mass measurements. The sensitivity of the balance used was 0.1 mg. Three measurements of weight gain at each time were taken and averaged. The oxidation behavior was evaluated by the weight gain of the samples.

Table 1
Plasma-sprayed parameters for bond coating and nano-13AlYSZ coating.

	NiCrAlY bond coating	13AlYSZ coating
Primary gas Ar (L/min)	60	60
Secondary gas H_2 (L/min)	20	15
Carrier gas Ar (L/min)	3.5	4.5
Gun current (A)	580	600
Gun voltage (V)	60	63
Spray distance (mm)	290	80
Powder feed rate (g/min)	45	25

2.4. Microstructure analysis

The nano-13AlYSZ coating before and after thermal cycling was characterized using a D/max 2200pc X-ray diffractometer (Cu Ka radiation; Rigaku, Tokyo, Japan). The microstructure of the nano-13AlYSZ coating was determined by an S-3500 scanning electron microscope (SEM, Hitachi, Tokyo, Japan) with energy dispersive X-ray spectroscopy (EDS).

2.5. Finite element analysis of TBCs

The FE analysis was calculated to determine detailed stress states in the test specimens coated with the TBCs as cooling to 20 °C from a stress-free state at 1100 °C using finite element code ANSYS 9.0 developed by ANSYS Inc., Canonsburgh, PA, USA.

2.5.1. Specimen geometry

The model consisted of four layers: substrate (3 mm), bond coat (0.1 mm), TGO and top coat (0.25 mm). The thickness of the TGO was set to 10 μm. The TBC/bond coat interface was modeled by a sinusoidal wavy interface with a wavelength of 200 μm and amplitude of 20 μm. The 2D four-node thermal-structure coupled-field solid element PLANE13 was selected. The specimen geometry is shown in Fig. 1. Path A is along the interface between the top coat and TGO. Path B is perpendicular surface of the top coating, from the top coating to the substrate at the edge of the coating.

2.5.2. Material properties

All layers were assumed to be homogeneous, isotropic and pure elastic. Creep and plastic deformation of each layer were assumed negligible. In addition, material properties used for substrate, bond coat, alumina and top coat were temperature

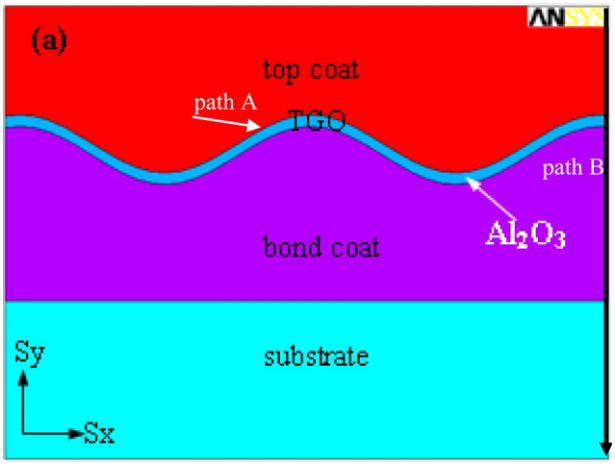

Fig. 1. The geometry model.

Table 2
Material properties of 13AlYSZ coating.

	Temperature (°C)	EX (10^9 Pa)	ALPX (10^{-6} °C^{-1})	Mass density (10^3 kg/m^3)	KXX (W/m °C)	*C* (J/kg °C)	PRXY
13AlYSZ	20	168	10.42	4.44	1.129	480	0.3
	300	162	10.85	4.44	1.108	620	0.3
	600	155	10.9	4.44	1.155	700	0.3
	900	149	10.93	4.44	1.181	760	0.3
	1200	140	10.98	4.44	1.249	810	0.3

dependent. Material properties of substrate, bond coat and alumina required for the model were derived from the literature [19]. The material properties of 13AlYSZ are shown in Table 2.

2.5.3. Boundary conditions and thermal loading

Because of the symmetry of specimen, an axisymmetric boundary condition was used. The boundary conditions and thermal loading were as follows:

(1) All layers were assumed to be stress free at 1100 °C.
(2) The upper surface of top coat transfers heat with air by convection; the side surface is thermal insulation; the creep and plastic deformation of all layers are negligible and was not taken into account.
(3) The system load was a cooling phase of 600 s from 1100 °C to 20 °C.
(4) The three-dimensional problem is reduced to a two dimensional one when the symmetry is considered.

The stress tends to generate in the cooling period of the thermal cycle. In this study, only the radial stress S_x and axial stress S_y of the coating were discussed (Fig. 1).

3. Results and discussion

The micrograph of cross-sectional microstructures of the nano-13AlYSZ coating is shown in Fig. 2. As shown in Fig. 2(a), the nano-13AlYSZ coating includes bond coat and ceramic coat, and the ranges of thickness of bond coat and ceramic coat is 80–100 μm and 200–250 μm, respectively. Fig. 2(b) demonstrates that the coating is mainly characterized by nano-zones (unmelted or partially melted particles), dense areas (melted area) and pores, which is typical of APS nanostructured coating. The size of the sprayed nanostructured particles is about 0.7 μm.

The nano-13AlYSZ coating before and after thermal cycling test was analyzed by X-ray diffraction. As shown in Fig. 3, t-ZrO_2 is the main phase and no m-ZrO_2 phase and α-Al_2O_3 are observed in the as-sprayed coating when the spallation extended to 5% area of the coating, in addition to strong peaks of tetragonal phase there are weak peaks of monoclinic phase and α-Al_2O_3 phase. It means that during thermal cycling at 1100 °C, the α-Al_2O_3 precipitates as a result of the outward diffusion of the Al that is in solid solution with ZrO_2 or detachment from the Al-rich amorphous phase. Meanwhile, there is a phase transformation during the thermal cycling, leading to the occurring of m-ZrO_2.

Fig. 4(a) shows the weight gain as a function of time for nano-13AlYSZ coating at 1100 °C in static air. In the early stage of the oxidation, the selective oxidation occurred, so the weight gain is higher. The weight gain is 1.63 mg/cm^2 after isothermal oxidation for 47 h. After about 71 h, the weight gain becomes flat. Finally the weight change per unit area was about 2.40 mg/cm^2 after isothermal oxidation for 147 h at 1100 °C.

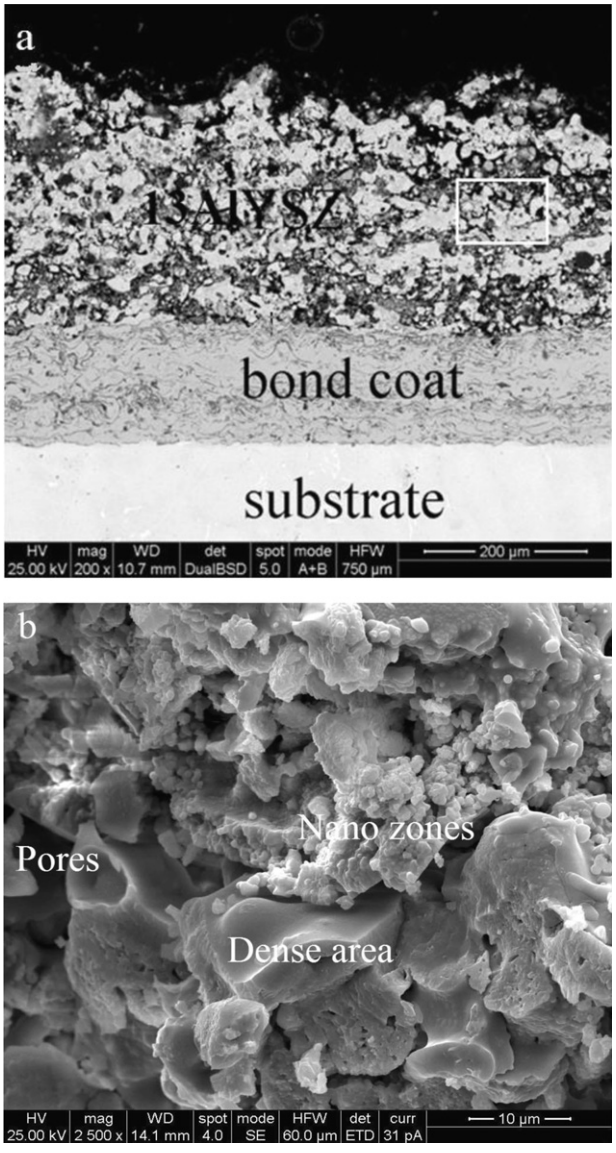

Fig. 2. Cross section (a) and the fractured cross section (b) of nano-13AlYSZ coating.

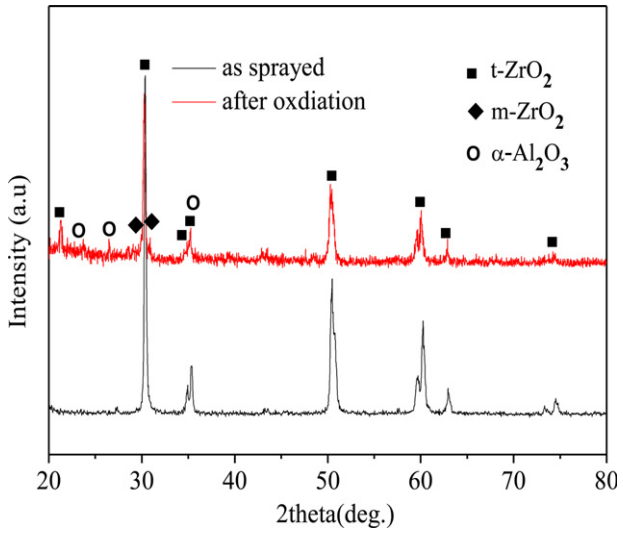

Fig. 3. XRD pattern of nano-13AlYSZ coating before and after oxidation.

The oxidation kinetics can be quantified further in terms of oxidation exponent n and rate constant k_p obtained from the relation:

$$\Delta W^n = k_p t \quad (1)$$

where ΔW is the weight change per unit area of the specimen and t is the exposure time. Fig. 4(b) shows the variation of log ΔW against log t for the nanostructured 13AlYSZ coating at 1100 °C. The slope of the nano-13AlYSZ coating sample is calculated as 0.52 ($n \approx 2$) in the log ΔW–log t plot. This means that the oxidation process of the nano-13AlYSZ coating obeys the parabolic rate law. The parabolic rate constant (k_p) at 1100 °C is calculated to be 0.04365 mg^2 cm^{-4} h^{-1}.

Fig. 5 is the cross-sectional SEM micrographs of nano-13AlYSZ coating along the bond coat and top coat interface after 953 cycles at 1100 °C, and corresponding elemental maps: O, Zr, Al, Y, Ni, Co and Cr. Element-distribution map analysis on the oxide formed in air revealed strong profile of Al and O, indicating that the oxide was mainly composed of Al_2O_3. Meanwhile, some Ni, Cr (Al) compound oxides also formed. A layer of Al_2O_3 and Ni, Cr (Al) compound oxides between the top coat and the bond coat may prevent the coating from further oxidation. It can be seen that the TBC with NiCrAlY bond coat failed by cracking at the interface between the TGO and the top coat. The failure of the nano-13AlYSZ coating is similar to the failure of conventional APS coating [20].

Fig. 6(a) shows a typical contour plot of radial stress (S_x) distribution of nano-13AlYSZ coating. It can be seen that the stresses in the radial (x) direction in both the TGO and nano-13AlYSZ top coat are compressive in nature. Maximum stresses occurred at the interface between the top coat and TGO. The maximum radial stresses for nano-13AlYSZ is about 3.88 GPa. The stresses in the axial (y) direction of nano-13AlYSZ coating are shown in Fig. 6(b). It can be seen that the maximum stresses occurred at the top coat/TGO interface. The maximum compressive stress is 496 MPa.

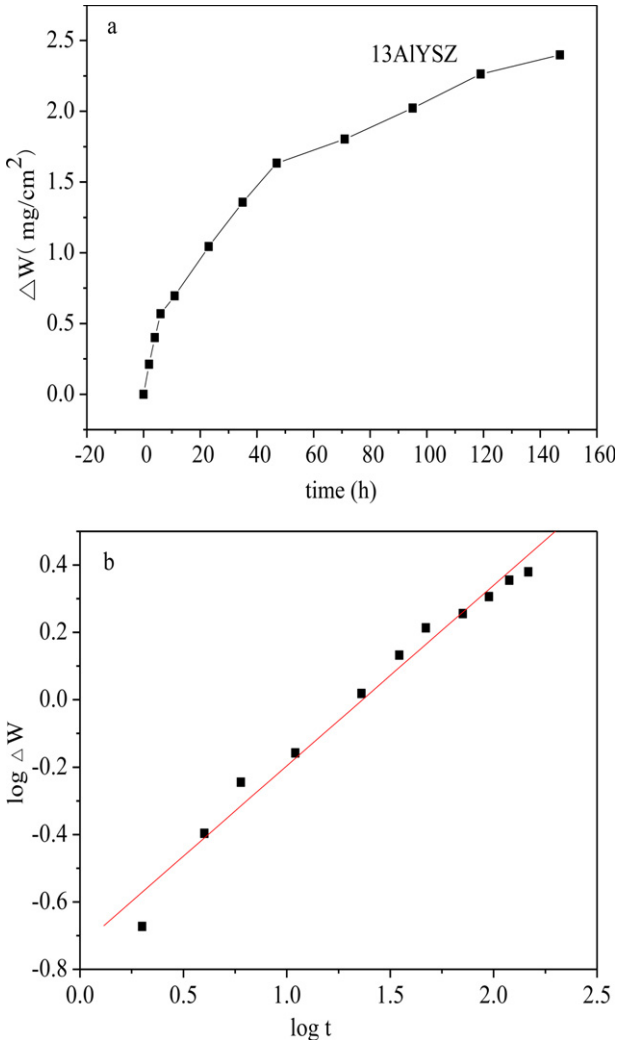

Fig. 4. Isothermal oxidation kinetics of nano-13AlYSZ coating at 1100 °C in static air (a) and (b) is the variation of logarithm of weight gain with logarithm of time.

Fig. 7 shows a comparison between radial (x) stress and axial (y) stress distribution along the top coat/TGO interface (path A) of nano-13AlYSZ coating. The stress (radial stress and axial stress) presented periodic distribution. Moreover, it can be seen that the radial (x) stress are both compressive in the concave and convex of the interface, while the tensile axial (y) stress in convex converges into compressive stress in concave. The maximum radial stresses for 13AlYSZ is 1.67 GPa. The tensile axial stresses in convex is 5 MPa, while that in concave is 32.6 MPa.

Fig. 8 shows the distribution of radial (x) stress and axial (y) stress of nano-13AlYSZ coating along the path B. It can be seen that the radial (x) stress in coating is compressive in nature. However, the axial (y) stress in both top coat and the TGO are tensile, whereas in bond coat and substrate is mainly compressive. The maximum tensile axial (y) stress occurred at the interface between the TGO and top coat at the edge of the specimen. The maximum axial stress for 13AlYSZ is 397 MPa, which may lead to the spallation of the nano-13AlYSZ coating between the top coat and the TGO during the thermal cycling.

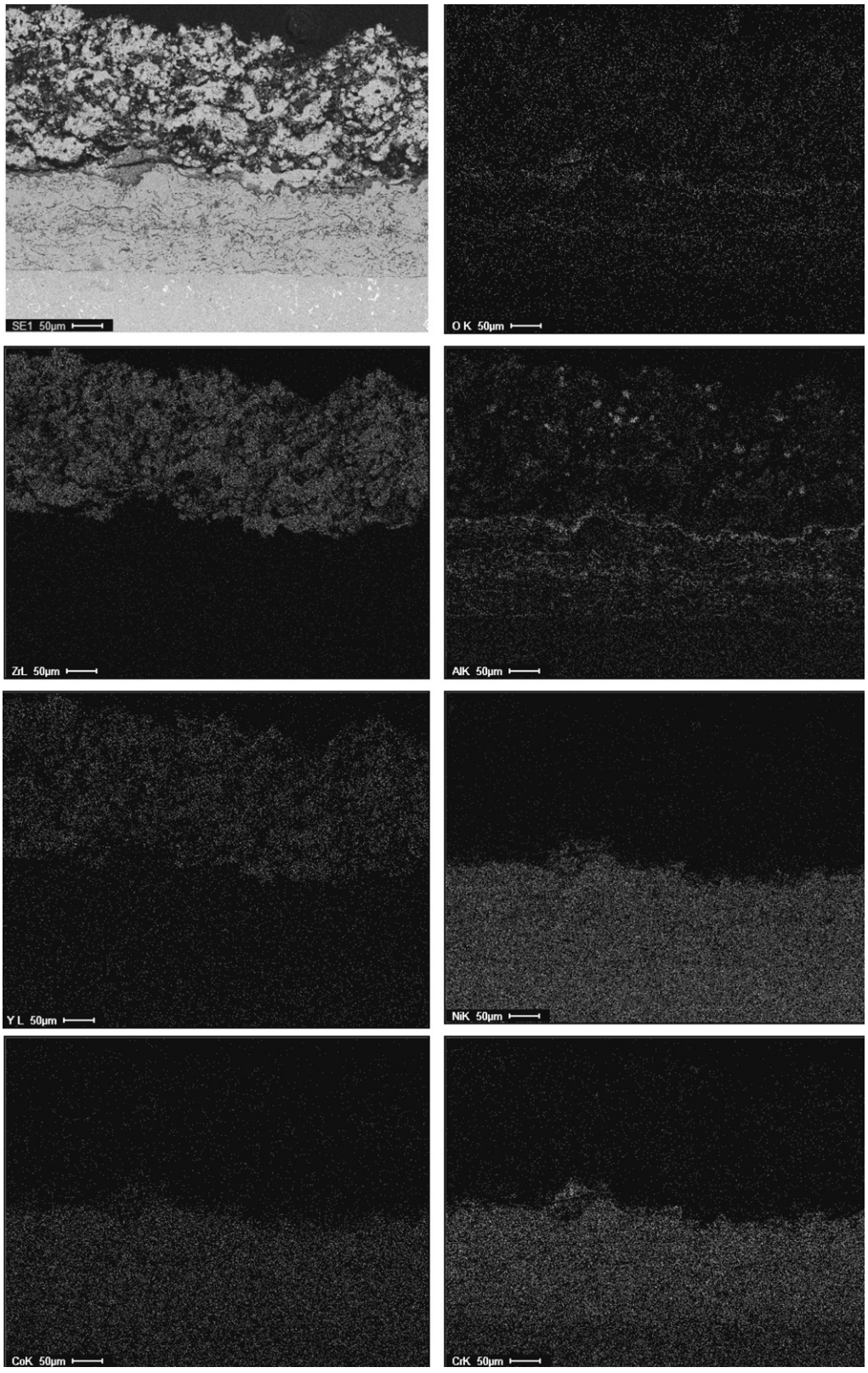

Fig. 5. Cross-sectional SEM micrograph of as-deposited nano-13AlYSZ coating after cyclic oxidation testing at 1100 °C for 953 cycles, and corresponding elemental maps: O, Zr, Al, Y, Ni, Co and Cr.

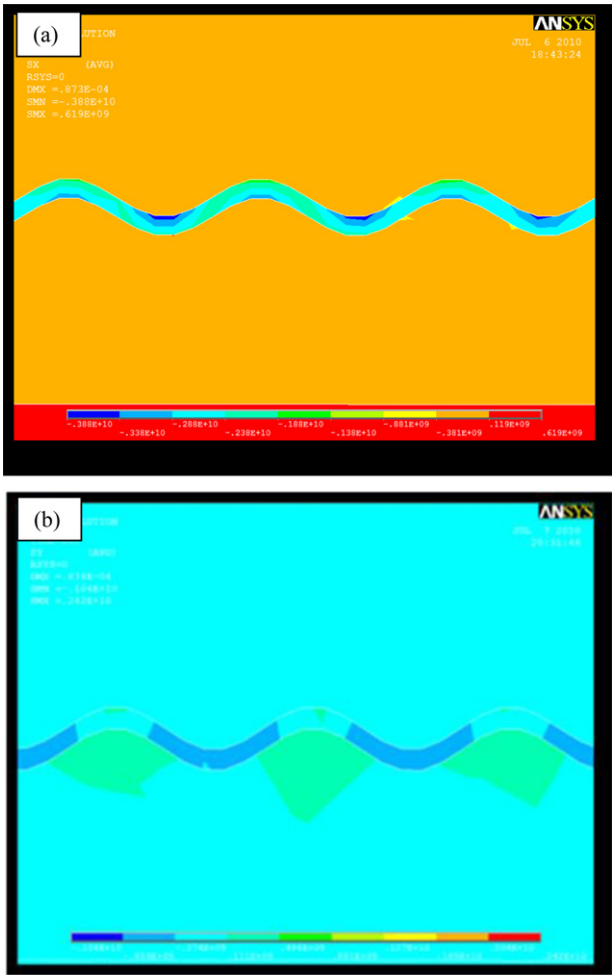

Fig. 6. Typical contour plot of radial stress S_x distribution (a) and axial stress S_y distribution (b) in nano-13AlYSZ coating.

It can be seen that the TBC with NiCrAlY bond coat failed by cracking at the interface between the TGO and the top coat (Fig. 5). The performance of plasma sprayed nano-13AlYSZ coatings during thermal cycling is related directly to the

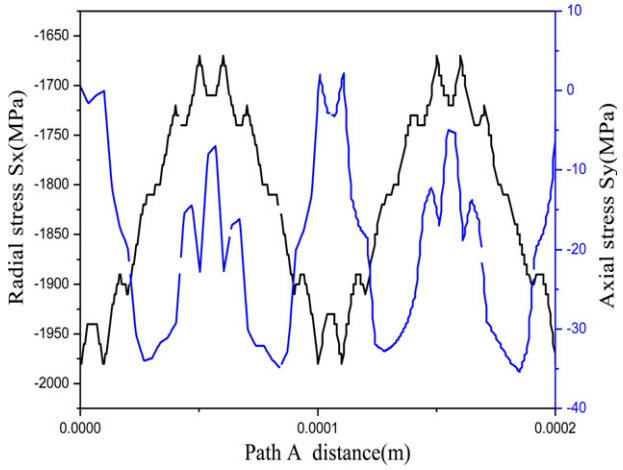

Fig. 7. Relation of radial and axial stress at the interface between the TGO and the nano-13AlYSZ top coat at the edge of the sample with time during the cooling to 20 °C from a stress-free state at 1100 °C.

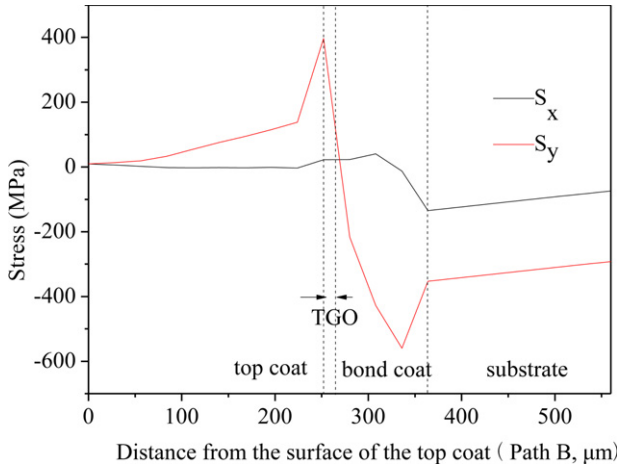

Fig. 8. Distribution of radial (x) stress and axial (y) stress of nano-13YSZ coating along the path B.

generation of thermal fatigue cracks due to thermal residual stress in the coatings. The stress in the radial (x) direction would lead to surface crack and unstable bending and the stress in the axial (y) direction along the interface between top coat and TGO at the edge of the sample is very important for breaking off the ceramic coat from the bond coat [21]. As shown in Fig. 6(a), the stresses in the radial (x) direction in both the TGO and nano-13AlYSZ top coat are compressive, leading to the unstable bending during the heat treatment. As confirmed by Figs. 6(b) and 8, the maximum compressive axial stresses of nano-13AlYSZ coating occurred along the top coat/TGO interface, causing the cracks between the TGO and top coating. The thermal cyclic life of nano-13AlYSZ coating is about 953 cycles. The thermal cycling life of the nano-13AlYSZ coating is higher than that of traditional YSZ coating (about 785 cycles) [18]. The nano-13AlYSZ (397 MPa) has relatively lower stress than that of traditional YSZ (517 MPa) [22]. The lower stress is that nano-coatings can absorb more residual stress and improve the strain tolerance. It could be concluded that lower stress in the nano-13AlYSZ coatings result in the higher thermal cycling life than that of conventional YSZ coating.

4. Conclusions

Effects of nano-Al_2O_3 addition on the isothermal oxidation and the thermal cycle life of nanostructured YSZ coating produced by APS were investigated. Weight gain of the TGO approximately followed a parabolic kinetics and the parabolic rate constant is 0.04365 $mg^2\,cm^{-4}\,h^{-1}$. The lifetime of the nano-13AlYSZ was about 953 times at 1100 °C. As confirmed by the finite element method, the failure of the nano-13AlYSZ coating occurred near the interface between the TGO and the top coat.

Acknowledgements

This work is supported by the National Natural Science Foundation of China, the Aviation Science Foundation of 2011ZF51062, Program for New Century Excellent Talents in

University (NCET) and Program for Changjiang Scholars and Innovative Research Team in University (IRT0512).

References

[1] Y. Zeng, S.W. Lee, L. Gao, C.X. Ding, Atmospheric plasma sprayed coatings of nanostructured zirconia, J. Eur. Ceram. Soc. 22 (2002) 347–351.
[2] R.S. Lima, A. Kucuk, C.C. Berndt, Evaluation of microhardness and elastic modulus of thermally sprayed nanostructured zirconia coatings, J. Surf. Coat. Technol. 135 (2001) 166–172.
[3] H. Chen, X.M. Zhou, C.X. Ding, Investigation of the thermomechanical properties of a plasma-sprayed nanostructured zirconia coating, J. Eur. Ceram. Soc. 23 (2003) 1449–1455.
[4] O. Racek, C.C. Berndt, Mechanical property variations within thermal barrier coatings, Surf. Coat. Technol. 202 (2007) 362–369.
[5] M. Gell, Application opportunities for nanostructured materials and coatings, Mater. Sci. Eng. A 204 (1995) 246–251.
[6] B. Liang, H.L. Liao, C.X. Ding, C. Coddet, Nanostructured zirconia–30 vol.% alumina composite coatings deposited by atmospheric plasma spraying, Thin Solid Films 484 (2005) 225–231.
[7] R.S. Lima, B.R. Marple, Nanostructured YSZ thermal barrier coatings engineered to counteract sintering effects, Mater. Sci. Eng. A 485 (2008) 182–193.
[8] N. Wang, C.G. Zhou, S.K. Gong, H.B. Xu, Heat treatment of nanostructured thermal barrier coating, Ceram. Int. 33 (2007) 1075–1081.
[9] R.W. Trice, Y.J. Su, J.R. Mawdsley, K.T. Faber, A.R.D. Arellano-López, H. Wang, W.D. Porter, Effect of heat treatment on phase stability, microstructure, and thermal conductivity of plasma-sprayed YSZ, J. Mater. Sci. 37 (2002) 2359–2365.
[10] A.L. Vasiliev, N.P. Padture, X.Q. Ma, Coatings of metastable ceramics deposited by solution-precursor plasma spray: I. Binary ZrO_2–Al_2O_3 system, Acta Mater. 54 (2006) 4913–4920.
[11] A.L. Vasiliev, N.P. Padture, Coatings of metastable ceramics deposited by solution-precursor plasma spray: II. Ternary ZrO_2–Y_2O_3–Al_2O_3 system, Acta Mater. 54 (2006) 4921–4928.
[12] M. Matsumoto, K. Aoyama, H. Matasubara, K. Takayama, T. Banno, Y. Kagiya, Y. Sugita, Thermal conductivity and phase stability of plasma sprayed ZrO_2–Y_2O_3–La_2O_3 coatings, Surf. Coat. Technol. 194 (2005) 31–35.
[13] K. An, K.S. Ravichandran, R.E. Dutton, S.L. Semiatin, Microstructure, texture, and thermal conductivity of single-layer and multilayer thermal barrier coatings of Y_2O_3-stabilized ZrO_2 and Al_2O_3 made by physical vapor deposition, J. Am. Ceram. Soc. 82 (1999) 399–406.
[14] Y. Liu, Y.F. Gao, S.Y. Tao, X.M. Zhou, H.J. Luo, La_2O_3-modified YSZ coatings: high-temperature stability and improved thermal barrier properties, Surf. Coat. Technol. 203 (2009) 1014–1019.
[15] M. Matsumoto, N. Yamaguchi, H. Matasubara, Low thermal conductivity and high temperature stability of ZrO_2–Y_2O_3–La_2O_3 coatings produced by electron beam PVD, Scr. Mater. 50 (2004) 867–871.
[16] M. Matsumoto, T. Kato, N. Yamaguchi, D. Yokoe, H. Matsubara, Thermal conductivity and thermal cycle life of La_2O_3 and HfO_2 doped ZrO_2–Y_2O_3 coatings produced by EB-PVD, Surf. Coat. Technol. 203 (2009) 2835–2840.
[17] Q.H. Yu, C.G. Zhou, H.Y. Zhang, F. Zhao, Thermal stability of nanostructured 13 wt.%Al_2O_3–8 wt.%Y_2O_3–ZrO_2 thermal barrier coatings, J. Eur. Ceram. Soc. 30 (2010) 889–897.
[18] Q.H. Yu, A. Rauf, C.G. Zhou, Microstructure and thermal properties of nanostructured 4 wt.%Al_2O_3–YSZ coatings produced by atmospheric plasma spraying, J. Therm. Spray Technol. 19 (2010) 1294–1300.
[19] M. Nishida, T. Hanabusa, H. Fujiwara, X-ray residual stress measurement of laminated coating layers produced by plasma spraying, Surf. Coat. Technol. 61 (1993) 47–51.
[20] G.C. Chang, W. Phucharoen, R.A. Miller, Finite element thermal stress solutions for thermal barrier coatings, Surf. Coat. Technol. 32 (1987) 307–325.
[21] K.A. Khor, Y.W. Gu, Effects of residual stress on the performance of plasma sprayed functionally graded ZrO_2/NiCoCrAlY coatings, Mater. Sci. Eng. A 277 (2000) 64–76.
[22] C.G. Zhou, N. Wang, H.B. Xu, Comparison of thermal cycling behavior of plasma-sprayed nanostructured and traditional thermal barrier coatings, Mater. Sci. Eng. A 452–453 (2007) 569–574.